Bull SJ. Size effects in the mechanical response of nanoscale multilayer coatings on glass. *Thin Solid Films* 2014, 571(Part 2), 290-295.

DOI link to article:

http://dx.doi.org/10.1016/j.tsf.2014.04.014

Date deposited:

15/05/2015

Embargo release date:

18 April 2014

Size effects in the mechanical response of nanoscale multilayer coatings on glass

S.J. Bull

Newcastle University

School of Chemical Engineering and Advanced Materials

Newcastle upon Tyne

NE1 7RU, UK

Abstract

Very thin (100-400 nm) oxide coatings which are used as antireflection and barrier layers in low emissivity architectural glass have been studied by nanoindentation methods to determine the effect of coating thickness on mechanical response. Whereas plasticity (hardness) is relatively easy to assess the elastic response of the coating is underestimated as the thickness is reduced. Thus, although some changes are observed with thickness, there is no size effect in elasticity. Size effects in plasticity are only observed for the crystalline layers such as ZnO whereas the other oxides deposited in this study were amorphous and show no size effect. Traditional microindentation-derived methods to determine the fracture toughness are unsuitable for assessing very thin coatings (<500 nm) and alternative energy-based models are required depending on what features are visible in indentation load-displacement curves. For oxide coatings no size effects in fracture toughness were observed, however

there are process-induced variations in residual stress which will affect the apparent fracture and adhesion strengths of the coatings. Failure by delamination during scratching depends on the magnitude of the applied stress which in turn depend on the thickness of coating layers deposited. This is because the friction tractions are controlled by the surface roughness which increases with coating thickness.

1. INTRODUCTION

For electronic and optical applications the design of coating-substrate systems has been predominantly controlled by their functional properties but more recently the mechanical response of the system has been used to enhance functional properties, as in the case of low emissivity coatings on architectural glass where scratch and damage resistance is a critical parameter in successful handling. As coatings become more complex, with multilayer and graded architectures now in widespread use, it is very important to obtain the mechanical properties (such as hardness, elastic modulus, fracture toughness, etc.) of individual coating layers for use in design calculations at the thickness present in the coating design since size-effects may be important in very thin layers (<1 μm).

For Bulk materials and sufficiently thick coatings standard methods to measure mechanical properties have been established including methods requiring the

manufacture of standard test pieces which can be machined from the bulk or indentation methods which are often easier to perform but give more scattered results [e.g.1-2]. The main testing methodologies for the assessment of bulk materials and thick coatings include bending, buckling, tensile, indentation, and scratch tests. As coating thickness is reduced and complex compositions and structures are introduced, it is difficult to use standard mechanical test methods to measure mechanical properties. Nanoindentation testing is often the only viable approach to assess the damage mechanisms and properties of such very thin coatings since it can operate at the required scale and provides a fingerprint of the indentation response of the coating/substrate system. If coating properties are to be assessed, the key point is to ensure any measured value is free from the influence of the deformation of the substrate or lower coating layers. Finite element analysis of indentation load displacement curves can be used to extract materials properties for design; as coating thicknesses decrease it is observed that the yield strength required to fit the curves increases and scale-dependent materials properties are essential for design [3]. However, this is a complex and time-consuming process and it is often easier to use simple analytic models to extract coating properties from coating/substrate system data, provided that this is of sufficient quality.

Relatively little is known about the mechanical properties of oxide coatings on architectural glass and there is also a need to determine if there are size effects

in fracture as well as plasticity as increasingly thinner coatings are used. This is the subject of this paper.

2. Experimental

2.1 Coatings investigated

Experiments were carried out on float glass, coated with the main layers in a multilayer stack of silver and metal oxides in a solar control configuration. A commercial coating consists of a 10 nm silver layer surrounded by SnO_2 and ZnO anti-reflection coatings and TiO_xN_y barrier layers; the layer structure and nominal coating thicknesses are presented in Table 1. A thin conducting ITO layer is used to prevent the silver layer from oxidation during the subsequent deposition of tin oxide. For the purposes of fracture and plasticity assessment of the individual oxide layer materials the previous coating layers were deposited according to the solar control coating design in Table 1 but the final coating layer was deposited to a range of thicknesses from 100 to 400 nm. This should ensure a similar microstructure is tested in each case.

The coatings were produced by sputtering in a commercial coating plant at Pilkington Technical Centre (Lathom, UK) using the same process parameters as used for commercially available solar control coatings from the same manufacturer (available with the trade name Optitherm). The glass substrates

were not heated prior to coating. The majority of the coatings were produced by reactive sputtering from metal targets using argon sputtering gas and an oxygen backfill to create a stoichiometric coating. Nitrogen was added to the backfill for the TiO_xN_y coatings and the ITO coatings were produced from an oxide target. Coating thickness was determined by ellipsometry and the stoichiometry and uniformity of coating composition with thickness was confirmed by x-ray photoelectron spectroscopy (XPS) which also revealed that the interfaces between layers were sharp with only limited mixing between layers.

X-ray diffraction studies showed that all of the coatings were amorphous except for the ZnO coatings which were poorly crystalline and had the Wurtzite structure. Given that sample heating only occurred from the sputtering plasma the deposition temperature is expected to be less than 100 ^oC where amorphous layers are produced due to limited adatom mobility. The intensity of the (002) Wurtzite peak for ZnO was about 50% of that for a fully crystalline coating of the same thickness deposited at temperatures above 200 ^oC indicating that the coating may be about 50% crystalline. Using the Scherrer formula [4] for grain size in terms of the x-ray peak broadening for (002) ZnO gave a 30±12 nm grain size for the 400 nm thick coating. Similar values were measured for thinner coatings.

The TiOxNy composition was found to be $TiO_{1.9}N_{0.1}$ by XPS. Since the coatings were sputtered from metal targets with an oxygen backfill containing a small

amount of nitrogen it is not surprising that the coating has a similar composition to the most thermodynamically stable titanium oxide, TiO_2. XPS revealed about 8 wt% Sn in the indium tin oxide coating which is consistent with the target composition (10% SnO_2: 90% In_2O_3).

2.2 Indentation testing approach

Indentation experiments were performed using Hysitron Triboindenter fitted with a new Berkovich indenter (tip-end radius 100nm) for plasticity assessment and a new cube corner indenter (tip end-radius 40nm) for fracture assessment. Tests were performed under displacement control since this has been shown to generate accurate fracture data in such coatings [5]. The system hardness and elastic modulus were determined by the standard Oliver and Pharr method [6] since these materials do not display significant pile-up or sink-in. Measurements were made at a range of contact scales in order to allow the extraction of coating-only properties using the extrapolation methods outlined in ISO 14577 [7]. The accuracy of the elastic modulus data for the coatings was checked by using a predictive model of the contact modulus, E, of a coated system developed previously [8, 9] where

$$E = \frac{1}{\frac{1}{E_C}\left[1-\frac{\pi a_0}{\pi a_0+2t_C}\right]+\frac{1}{E_S}\left[\frac{\pi a_0}{\pi a_0+2t_C}-\frac{\pi a_0}{\pi a_0+2(t_C+t_S)}\right]} \quad (1)$$

Here E_c and E_s are the contact moduli of coating and substrate respectively, a_0 is the contact radius (determined from the contact area $A_c=\pi a_0^2$), t_c is the coating thickness and t_s is the substrate thickness. From this formulation it is clear that as a_0 tends to zero the value of E tends to E_c and that if a_0 is very much greater than t_c and t_s is much greater than a_0 then E tends to E_s as might be expected.

The ISO14577 extrapolation method was used on the contact modulus prediction from equation (1) as a function of contact depth to determine the expected modulus for a given coating material at different thicknesses to compare with experimental measurements. An example of this is shown in Figure 1 indicating that the fit gives an accurate modulus value for high coating thickness but that the fitted value is reduced as the coating thickness drops to 100 nm.

2.3 Fracture toughness assessment

Cube corner indentations have been performed in all oxide coatings tested here and generate fracture in the coatings. Depending on the coating material both picture frame and radial cracks were observed to form. When radial cracks were observed for the TO_xN_y, SnO_2 and ITO layers there were well defined features in the load-displacement curve (load drops since under displacement control) and the wp-dp method could be used for analysis [5, 10]. At higher loads in these coatings picture frame cracks formed and once these were well-established, the picture frame crack method [10, 11] could be used to determine critical strain

energy release rates. For ZnO layers this is the only practicable way to obtain such data. A reasonable agreement between the toughness values calculated by either approach has been observed previously [10].

2.4 Residual stress measurement

Most of the oxide coatings investigated were amorphous as far as x-ray diffraction was concerned. For this reason residual stress was measured from the changes in curvature of coated samples after deposition using the Stoney equation [12]. A thin (100 μm) glass substrate was used for the TiOxNy coatings where the residual stresses were low but the normal 4.2 mm thick substrate was used in for the other coatings. Stresses were checked using x-ray diffraction (XRD) for the thickest ZnO coating using the $\sin^2\psi$ method [13] since this was the only sufficiently crystalline material to be amenable to the analysis and a good agreement between XRD and curvature stress values was observed here (both 1±0.1 GPa compressive for the 200 nm ZnO coating).

2.5 Measurement of friction

Friction measurements between coated surfaces and PMMA spheres of 80 μm diameter were undertaken using a Hysitron Triboindenter. The sphere was attached to a holder with a cyanoacrylate adhesive and scratches were undertaken at a fixed normal load of 1mN over a scratch length of 10 μm.

3. Results and Discussion

3.1 Size effects in plasticity

Hardness (and elasticity) data was obtained at a range of contact scales for coatings in the thickness range 100-400 nm and extrapolated to zero thickness to give an indication of the coating only properties (Fig. 2). For most of the oxide coatings studied there is no appreciable plasticity size effect, though for zinc oxide the hardness does increase at lower coating thickness. This is probably related to the fact that all the deposited oxide coatings are poorly crystalline except for the ZnO and scale-dependent plasticity mechanisms, such as geometrically necessary dislocations [14, 15] require the presence of dislocations on well-defined slip planes which are not present in amorphous layers.

For the elastic properties the coating moduli are apparently independent of thickness within experimental error (Figure 2b). However, when using the ISO14577 extrapolation there is a tendency to underestimate the true coating properties as the coating thickness is reduced; this is due to the long range of elastic stresses leading to significant elastic contributions from the substrate even at very low contact depths. The model predictions here demonstrate this very well and provide an excellent match to the mean values of the experimental data for the same coating materials. Coatings should be at least 200 nm in

thickness for these slightly stiffer coatings on glass in order that the errors introduced by using the ISO14577 approach are low enough (<3%).

3.2 Size effects in fracture

Coatings of the same material with different thickness can show different mean fracture loads in indentation testing and it might be expected that this is due to differences in fracture toughness. However, for coatings in the thickness range 100-400 nm no size effects were observed (Fig. 3). Assuming pure mode I loading the critical strain energy release rates can be converted to fracture toughness values using

$$K_{Ic} = \sqrt{EG_c} \qquad (2)$$

Results of this calculation are presented in Table 2 and are comparable to data from bulk samples of the same materials obtained using conventional toughness tests [16].

Some workers have reported size effects in the fracture of oxide nanoparticles [e.g. 15] but these are typically much less than 100nm in diameter. The mechanisms used to describe such size-dependent fracture events are often related to the effects of local plasticity in the region of the crack tip – given the

lack of size effects in plasticity in these predominantly amorphous coatings the lack of a size effect in fracture is therefore not surprising.

Differences in fracture behaviour will depend on the stresses driving the fracture process and the distribution of defects in the coating as well as on the fracture toughness. Careful analysis of the coatings by AFM and transmission electron microscopy reveals poorly crystalline layers with few defects and none of the dislocations that are required for dislocation shielding based models for size effects in toughness [17]. There thus remains the question of what is the critical defect responsible for fracture.

The critical crack size, c, can be estimated from

$$K_{Ic} = \sigma\sqrt{\pi c} \qquad (3)$$

where σ is the tensile stress opening the crack. This stress will be the combination of the residual stress in the coating and the stress introduced by the indentation process. Table 2 shows measured values of residual stress in the coating (using the curvature method [12]). Table 2 also shows the stresses in the coating at the location of failure determined by finite element analysis of an indenter pressed into the coated sample with the fracture load; for details of the modelling approach see [18, 19]. The residual stress must be added to the indentation-induced stress to get a complete description of the stresses

responsible for failure; it is variations in this residual stress contribution which give rise to the apparent size effects in fracture strength seen in these coatings (see next section).

The critical crack sizes determined using equation (3) in this table are of a similar size to the surface roughness of the coatings and it is probable that the cracks are formed from surface roughness features. Since the surface roughness of the coatings increases with thickness (see section 3.4) it might be expected that the fracture stress will increase with thickness as well. However, the observed behaviour is much more variable and is controlled by changes in residual stress in the layers as discussed in the next section.

3.3 Size effects, residual stress and structure

Multilayer coatings develop a complex residual stress pattern with different contributions for the stresses generated in each individual layer. Due to differences in deposition conditions there are changes in residual stress with coating thickness observed in many coating systems. Generally, when very thin coatings are initially deposited on glass they are discontinuous and tensile stresses are generated which are a maximum at the point of coalescence [20]. Energetic coating processes such as sputtering are required to produce dense, compact coatings and also tend to produce coatings with intrinsic compressive stresses which counteract the initial tensile stresses. The magnitude of these

compressive stresses depends on the energy of ion bombardment and the stress relaxation processes which occur during deposition [21]. Finally thermal expansion mismatch stresses must be added to the total stress in the coating. These are generally developed on cooling from the deposition temperature at the end of the coating cycle but may develop during coating if the substrate temperature changes.

Figure 4 shows the stress measured in coated samples at the end of the deposition cycle for coatings of different thickness deposited with the same coating parameters onto a glass substrate coated with the usual underlayers in a solar control coating stack. The compressive stress in the TiOxNy is relatively low and does not change with coating thickness. In this case the thermal expansion mismatch stress is very low and the growth stress in the amorphous coating is constant at around 220 MPa compressive. Stress relaxation by viscoelastic or fracture processes can act to reduce the stress during deposition or subsequent annealing [22]. In the case of the ZnO the compressive stress in thin coatings is much higher than in thicker layers. In this case the thermal stress is about 180 MPa compressive and a much larger intrinsic growth stress is produced during deposition. The ZnO coating is the most crystalline of the layers investigated and shows higher hardness for thinner layers and less stress relaxation during deposition. Thinner layers with their finer grain size can support a higher residual stress than the thicker layers where some plastic deformation will occur. The ITO coating shows the highest compressive residual stress which

is dominated by a very high intrinsic growth stress (~3 GPa) caused by relatively intense ion bombardment during coating growth. This stress does not relax during deposition. The increase in residual stress with thickness is due to the temperature rise during deposition caused by this ion bombardment – the substrate temperature does not stabilise but continues to rise during deposition due to the poor thermal conductivity of the glass substrate.

3.4 Resistance to scratching

Coated glass is used in many applications where the glass is coated in one location and delivered to another for assembly into products such as windows. It therefore has to withstand the interaction with its environment during delivery and service. In the case of coated architectural glass one of the most serious potential failure modes is the formation of transit scratches during delivery – visible defects are most likely to be produced when the coatings are detached (Figure 5a). To reduce the possibility of damage to the coated glass surface PMMA spheres are sprayed over the coating to separate the glass sheets during transport. Despite this it is still possible for the spheres to slide over the coating during transport and cause detachment if the density of spheres is not high enough. Detachment often occurs initially due to the compressive stresses ahead of the sliding sphere (Figure 5b) but is often followed by through-thickness cracking in the detached zone and stripping of all or part of the coating with further sphere movement [23]. In the case of the solar control coating

investigated here it is adhesion failure at the ZnO/Ag interface which starts the process.

Since there is no spontaneous delamination the compressive residual stress in the coating alone is not sufficient to drive the buckling failure ahead of the contact. In this case there needs to be a further contribution from stresses generated by the friction in the contact. The friction behaviour of the TiOxNy top layer as a function of thickness for recently cleaned and contaminated surfaces left in laboratory air for 24 h is shown in Figure 6. There is a slight increase in the measured friction due to an increase in surface roughness for the clean surfaces but the contaminated surfaces show a constant lower friction value. The importance of the increase in friction with roughness was confirmed by analysing different regions of the 400 nm thick coating close to the sample edge where roughness variations were observed (Figure 7).

Using a simple Hertzian stress analysis with the elastic properties of the substrate alone [24] the maximum compressive stress in the coating ahead of the moving sphere is 250 MPa when the coefficient of friction is 0.3 and 450 MPa when the coefficient of friction is 0.6. These may be underestimates by as much as a factor of two given the higher elastic moduli of the coatings but are of the correct order of magnitude. The average residual stress in the multilayer coating is around 1.5 GPa so this dominates the detachment process. The stresses which cause detachment are much lower than those which lead to through-

thickness cracking so it is not surprising that the blistering is observed in Figure 5b.

In the worst case scenario the stresses responsible for delamination are about 1.95 GPa and taking a typical interfacial toughness of 1.9 $MPam^{1/2}$ the typical interfacial defect radius is 300 nm, very much larger than the total multilayer coating stack thickness. Figure 8 shows the defects visible in a detached region of a simulated transit scratch in the Pilkington Optitherm coating. The minimum defect diameter observed is about 600nm which agrees with this simple calculation. One such defect occurs in the Ag/ZnO interface every 100 μm^2 which is a very low defect density. Allowing the coating to contaminate and reduce friction can increase the critical defect size by 25%.

The defects responsible for detachment may have been present in the glass initially and have propagated through to the weak ZnO/Ag interface. However, it may be that Hydrogen weakens this interface [25, 26] and arises from the residual water in the deposition chamber during coating manufacture or from environmental exposure during service [27].

5. CONCLUSIONS

Nanoindentation testing can be used to determine a number of different mechanical properties of thin oxide coatings on glass which are necessary to

understand coating performance and, in particular, the mechanics of coating detachment in multilayer optical coatings which is a major failure mode. Since plasticity effects are highly localised it is possible to reliably determine the hardness response of oxide coatings on glass at thicknesses down to 100 nm. The longer range effects of elasticity mean that coatings need to be more than 200 nm thick if coating properties are to be reliably assessed. Although some changes in elastic modulus are observed with thickness, there is no size effect in elasticity. Size effects in plasticity are only observed for crystalline layers such as ZnO whereas the other amorphous oxides deposited in this study show no size effect.

Traditional microindentation-derived methods to determine the fracture toughness are unsuitable for assessing very thin coatings (<500 nm) and alternative energy-based models are required depending on what features are visible in indentation load-displacement curves. For oxide coatings no size effects in fracture toughness were observed, however there are process-induced variations in residual stress which will affect the apparent fracture and adhesion strength of the coatings. The failure stress driving delamination during scratching depends on the magnitude of the residual and applied stress; the latter in turn depends on the thickness of coating layers deposited. This is because the frictional surface tractions are controlled by the surface roughness which increases with coating thickness. Smoother coatings show low friction and are less likely to show delamination. Coatings which are contaminated by water and

hydrocarbons from the atmosphere also show a lower friction coefficient and a lower chance of failure. This has implications in the storage and delivery of newly coated glass.

ACKNOWLEDGEMENTS

This work was supported by EPSRC through the multiscale modelling initiative. Paul Warren at Pilkington plc is thanked for providing samples, some data and useful discussions.

References

1. B.R. Lawn, A.G. Evans and D.B. Marshall, “Elastic/Plastic Indentation Damage in Ceramics: The Median/Radial Crack System,” J. Am. Ceram. Soc., **63** (1980) 574-581.

2. G. R. Anstis, P. Chantikul, B.R. Lawn and D.B. Marshall, “A critical evaluation or indentation techniques for measuring fracture toughness: Part 1 Direct crack measurements, Part 2 Strength method,” J. Am. Ceram. Soc., **64** (1981) 533-538; 539-543.

3. S. Soare, S.J. Bull, A. Oila, A.G. O’Neill, N.G. Wright, A. Horsfall and J.M.M. dos Santos, “Obtaining mechanical parameters for metallisation stress sensor design using nanoindentation,” Z. Metall., **96** (2005) 1262-1266.

4. A. Patterson, "The Scherrer Formula for X-Ray Particle Size Determination". *Phys. Rev.* **56** (1939) 978–982.

5. J. Chen and S.J. Bull, “Assessment of the toughness of thin coatings using nanoindentation under displacement control,” Thin Solid Films, **494** (2006) 1-7.

6. W.C. Oliver and G.M. Pharr, “An improved technique for determining hardness and elastic modulus using load and displacement sensing indentation experiments,” J. Mater. Res., **7** (1992) 1564-1583.

7. ISO14577 part 4 “Metallic materials. Instrumented indentation test for hardness and materials parameters. Test method for metallic and non-metallic coatings,” (2007).

8. S.J. Bull, “Mechanical response of ALD alumina coatings on stiff and compliant substrates,” J. Vac. Sci. Technol., **A30** (2012) 01A1690.

9. S.J. Bull, “A simple method for the assessment of the contact modulus for coated systems,” Phil. Mag., in press (2014).

10. J. Chen and S.J Bull, “Indentation fracture and toughness assessment for thin optical coatings on glass,” J. Phys. D: Appl. Phys., 40 (2007) 5401-5417.

11. S.J. Bull, “Analysis methods and size effects in the indentation fracture toughness assessment of very thin oxide coatings on glass,” Comptes Rendue Mechanique, **339** (2011) 518-531.

12. J.A. Sue, “Stress determination for coatings,” in ASM Handbook Volume 5: Surface Engineering, ASM International , Metals Park Ohio, 1994, pp647-653

13. B.D. Cullity, “Elements of x-ray diffraction,” Addison-Wesley, 1978.

14. S.J. Bull,“On the origins and mechanisms of the indentation size effect,” Z. Metall., **94** (2003) 787-792.

15. W.W. Gerberich, W.M. Mook, C.B. Carter and R. Ballinari, “A crack extension force correlation for hard materials,” Int. J. Fracture, **148** (2007) 109-114.

16. “Engineering Property Data on Selected Ceramics Volume III, Single Oxides,” Metals and Ceramics Information Centre, Columbus, Ohio, (1981).

17. Y. Katz, R. Keller, H. Huang and W.W. Gerberich,“A dislocation shielding model for fracture of semibrittle polycrystals,“ Metall. Trans., **A24** (1993) 343-350.

18. J. Chen and S.J. Bull, “A critical examination of the relationship between plastic deformation zone size and Young’s Modulus to hardness ratio in indentation testing,” J Mater. Res., **21** (2006) 2617-2627.

19. J. Chen and S.J. Bull, “Finite element analysis of contact induced adhesion failure in multilayer coatings with weak interfaces,” Thin Solid Films, **517** (2009) 3704-3711.

20. H. Windischmann, “Intrinsic stress in sputter-deposited thin films,” Critical Reviews in Solid State and Materials Sciences, **17** (1992) 547-596.

21. S.J. Bull, A.M. Jones, and A.R. McCabe, “Residual stress in Ion Assisted Coatings,” Surf. Coat. Technol., **54/55** (1992) 173-179.

22. M.D. Thouless, “Modelling the generation and relaxation of stresses in films,” Ann. Rev. Mater. Sci., **25** (1995) 69-96.

23. K.J. Belde and S.J. Bull, “Intentional polymer particle contamination and the simulation of adhesion failure in transit scratches in ultra-thin solar control coatings on glass,” J. Adhesion Sci. Technol., **22** (2008) 121-132.

24. G.M. Hamilton and L.E. Goodman, “The stress field created by a circular sliding contact,” J. Appl. Mech., **37** (1966) 371-376.

25. E. Ando and M. Miyazaki, “Moisture resistance of the low-emissivity coatings with a layer structure of Al-doped ZnO/Ag/Al-doped ZnO,” Thin Solid Films, **392** (2001) 289-293.

26. J. Chen, Z. Lin, S.J. Bull, C.L. Phillips and P.D. Bristowe, “Experimental and modelling techniques for assessing the adhesion of very thin coatings on glass,” J. Phys. D: Appl. Phys. **42** (2009) 214003.

27. K.J. Belde and S.J. Bull, “Chemomechanical effects in optical coating systems,” Thin Solid Films, **515** (2006) 859–865.

Tables

Table 1: Structure of the multilayer coatings investigated

Position in the coating stack	Layer Material	Nominal thickness (nm)
Outermost barrier coating	TiO_xN_y	10
Outer AR coating	SnO_2	40
Protective layer	ITO	2
Wavelength selective layer	Silver	10
Inner AR layer	ZnO	10
Inner barrier layer	TiO_xN_y	20
Substrate	Float glass (air side coated)	4200000

Table 2: Stresses, fracture toughness and critical crack size for the 400nm thick coatings investigated in this study.

Coating	Residual stress, σ_r (GPa)	Indentation stress, σ_a (GPa)	Coating Youngs Modulus, E (GPa)	Coating fracture toughness, K_{iC} ($MPam^{1/2}$)	Critical crack size, c (nm)	Ra (nm)
TiO_xN_y	-0.2	12.2	122	1.8	7.2	9.1
ZnO	-1.0	11.7	117	1.1	3.4	12.7
ITO	-3.0	13.1	141	2.2	15.1	6.6
SnO_2	-3.0	13.3	133	1.9	10.8	8.6

Figure Captions

Fig. 1: Variation of contact modulus with contact radius for 100nm and 400nm thickness tin oxide coatings on glass (E_c=139GPa). The ISO 14577 fit is shown for comparison.

Fig. 2: (a) Hardness and (b) Young's Modulus determined by nanoindentation as a function of coating thickness.

Fig. 3: Strain energy release rate as a function of coating thickness for oxide coatings on glass determined by the wp-dp and picture frame crack methods [10,11].

Fig.4: Residual stress as a function of thickness for three different components of a solar control multilayer stack on glass.

Fig. 5: (a) Transit scratch in solar control coating and (b) initial stages of scratch formation by buckling in a single pass scratch test in the laboratory using a PMMA sphere indenter.

Fig. 6: Variation of friction coefficient with coating thickness for an 80μm diameter PMMA ball sliding on TiOxNy coated glass with a 1mN normal load.

Fig. 7: Variation of coefficient of friction with TiOxNy roughness determined from an AFM scan with a 10μm by 10μm area on different regions near the edge of a 400nm thick coated sample.

Fig. 8: Reflected light micrograph showing defects in the Ag/ZnO interfaces revealed in a simulated transit scratch in Pilkington Optitherm.

Figures

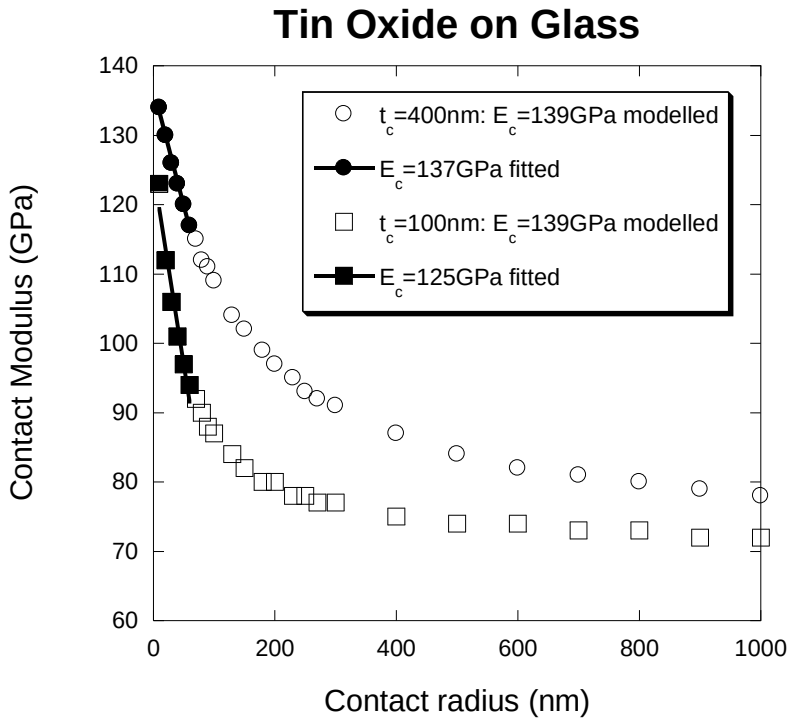

Fig. 1: Variation of contact modulus with contact radius for 100nm and 400nm thickness tin oxide coatings on glass (E_c=139GPa). The ISO 14577 fit is shown for comparison.

(a)

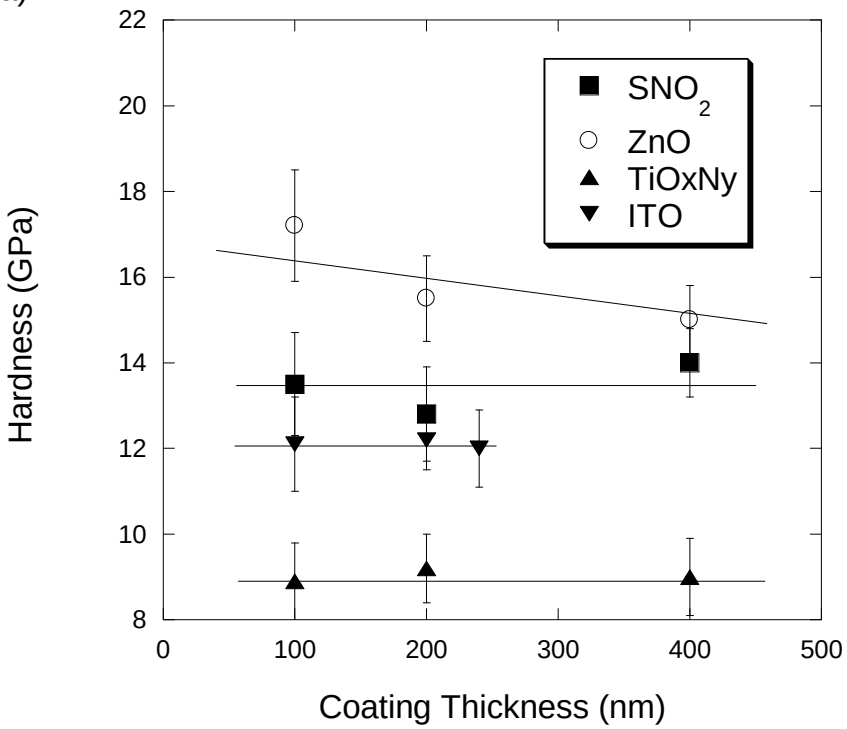

Fig. 2: (a) Hardness and (b) Young's Modulus determined by nanoindentation as a function of coating thickness.

(b)

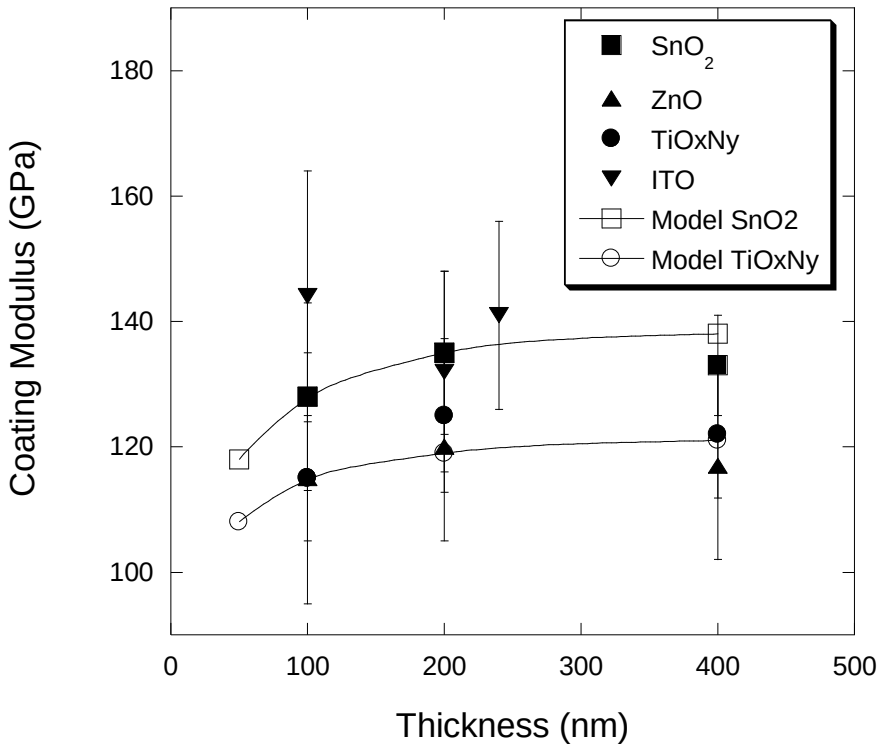

Fig. 2: (a) Hardness and (b) Young's Modulus determined by nanoindentation as a function of coating thickness.

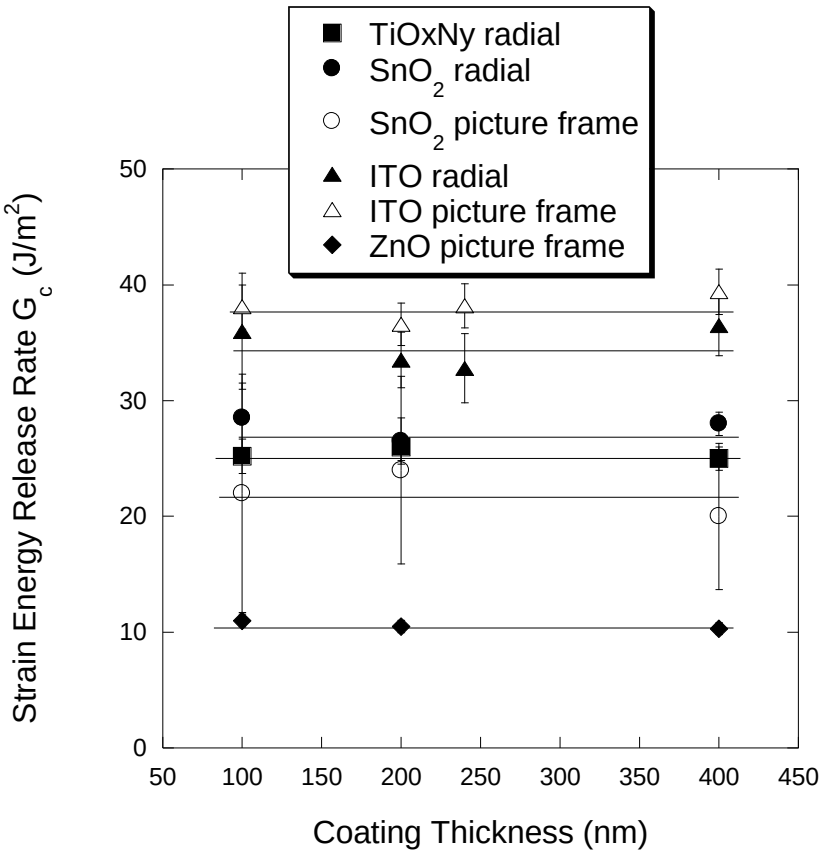

Fig. 3: Strain energy release rate as a function of coating thickness for oxide coatings on glass determined by the wp-dp and picture frame crack methods [9,10].

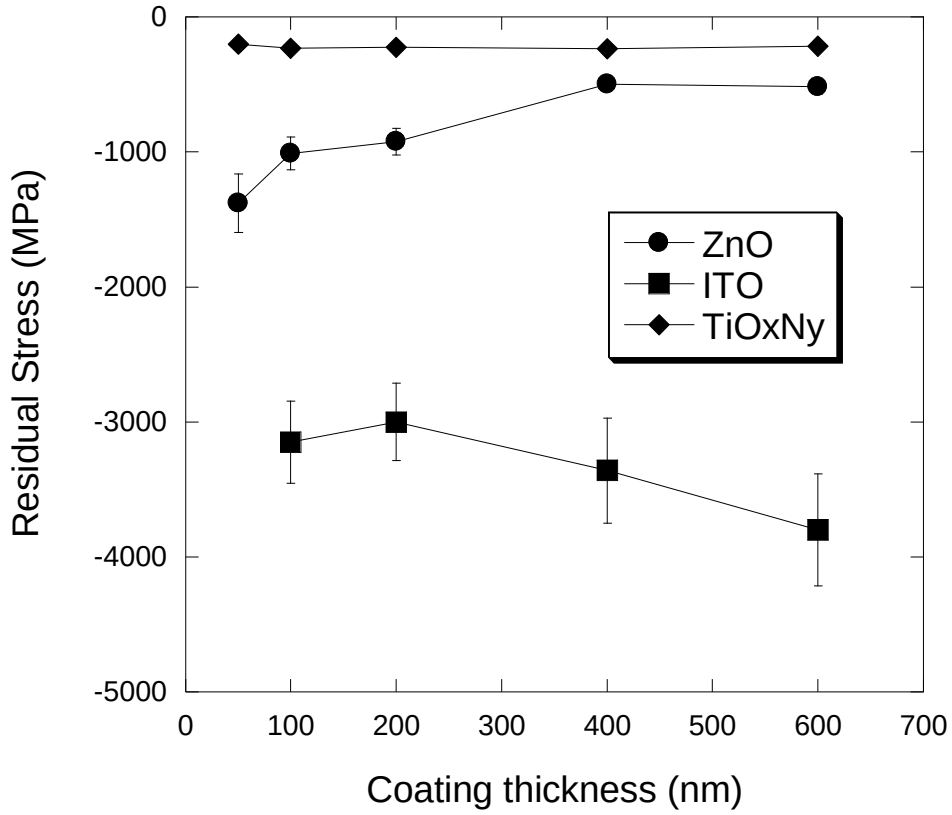

Fig.4: Residual stress as a function of thickness for three different components of a solar control multilayer stack on glass.

(a)

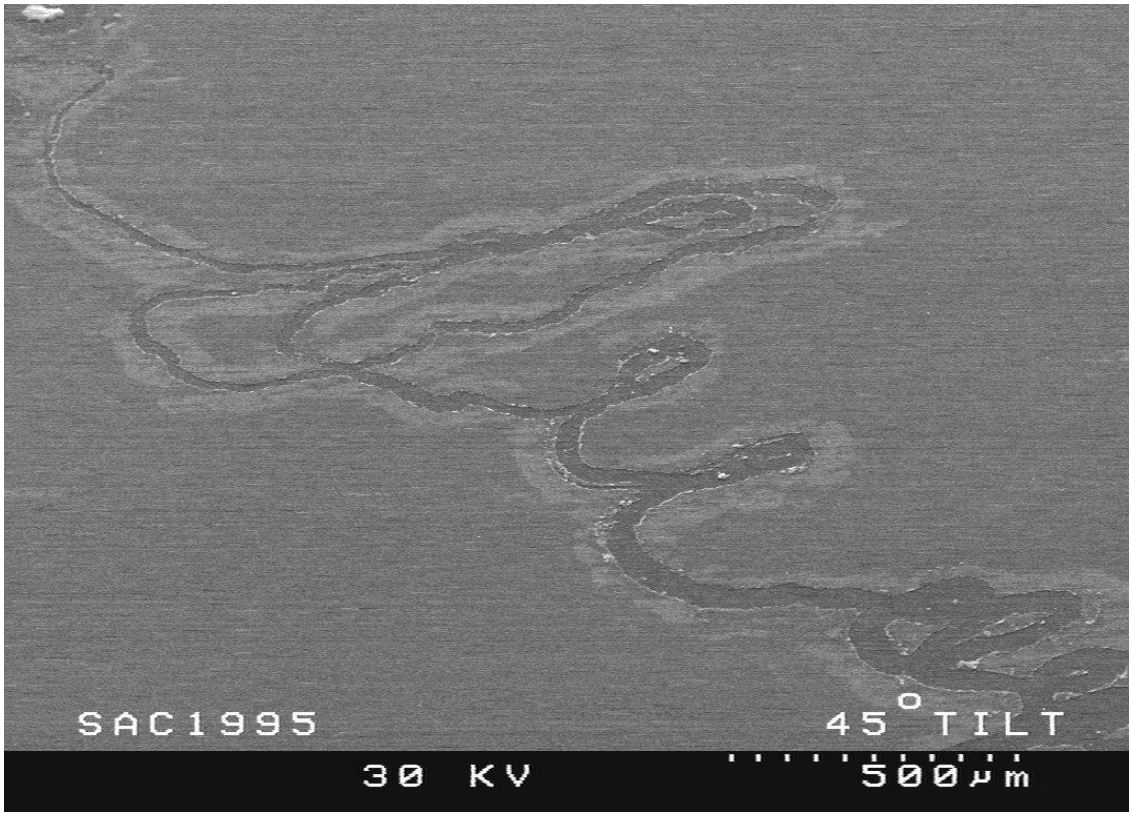

Fig. 5: (a) Transit scratch in solar control coating and (b) initial stages of scratch formation by buckling in a single pass scratch test in the laboratory using a PMMA sphere indenter.

(b)

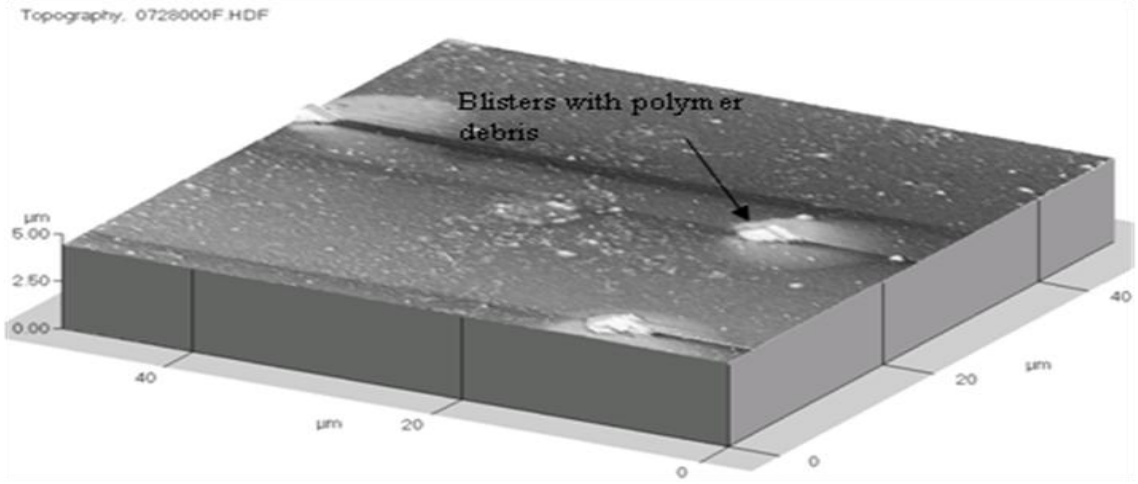

Fig. 5: (a) Transit scratch in solar control coating and (b) initial stages of scratch formation by buckling in a single pass scratch test in the laboratory using a PMMA sphere indenter.

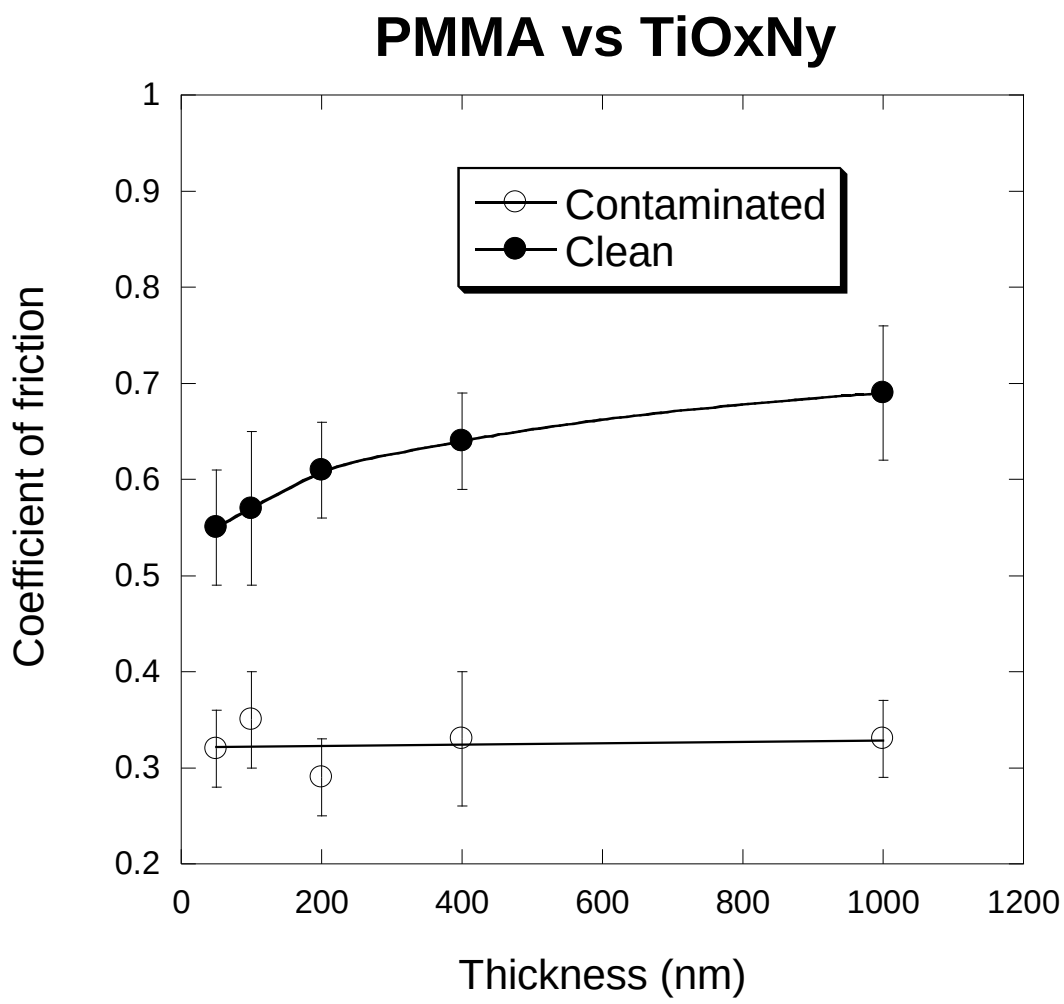

Fig. 6: Variation of friction coefficient with coating thickness for an 80μm diameter PMMA ball sliding on TiOxNy coated glass with a 1mN normal load.

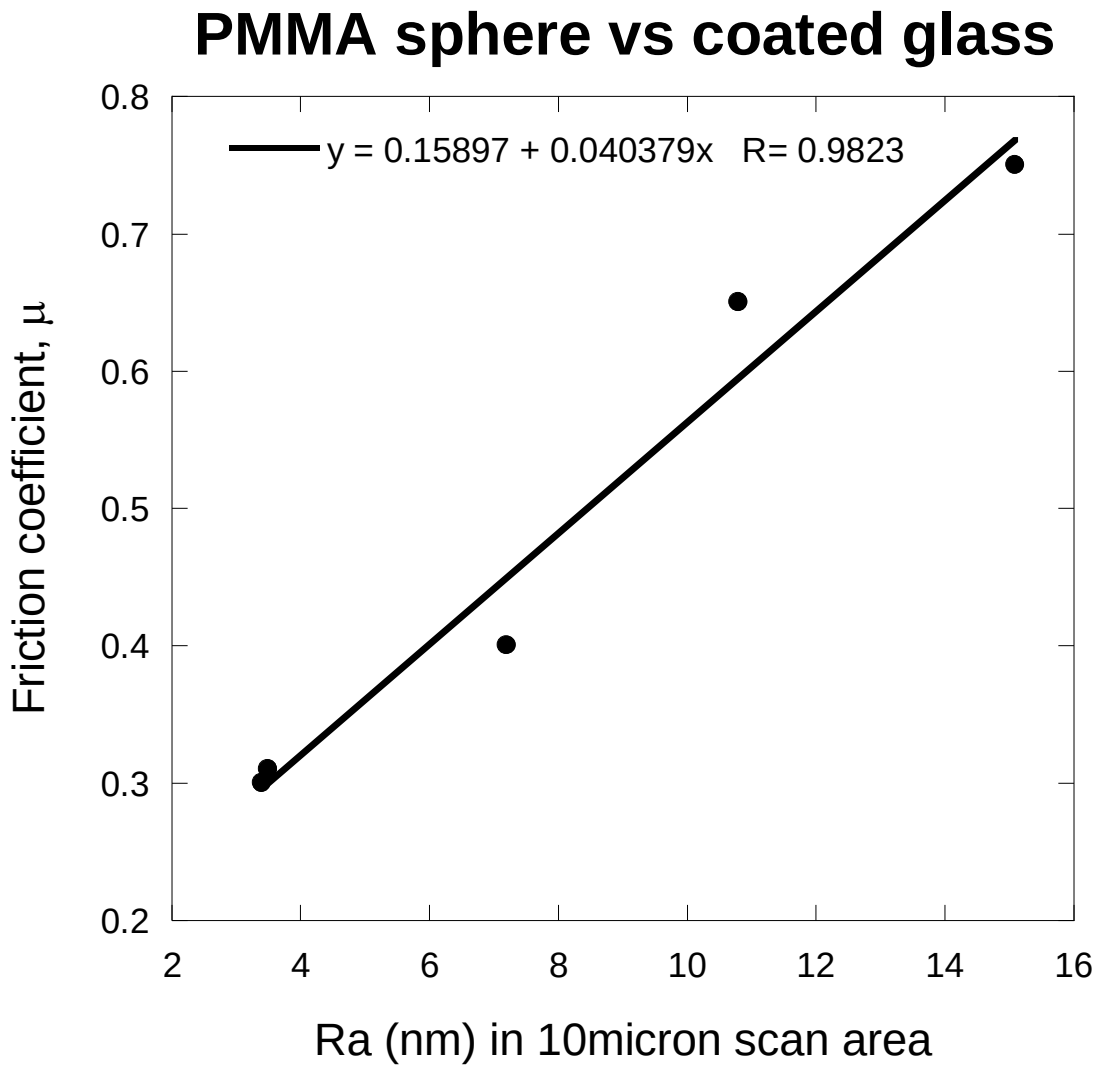

Fig. 7: Variation of coefficient of friction with TiOxNy roughness determined from an AFM scan with a 10μm by 10μm area on different regions near the edge of a 400nm thick coated sample.

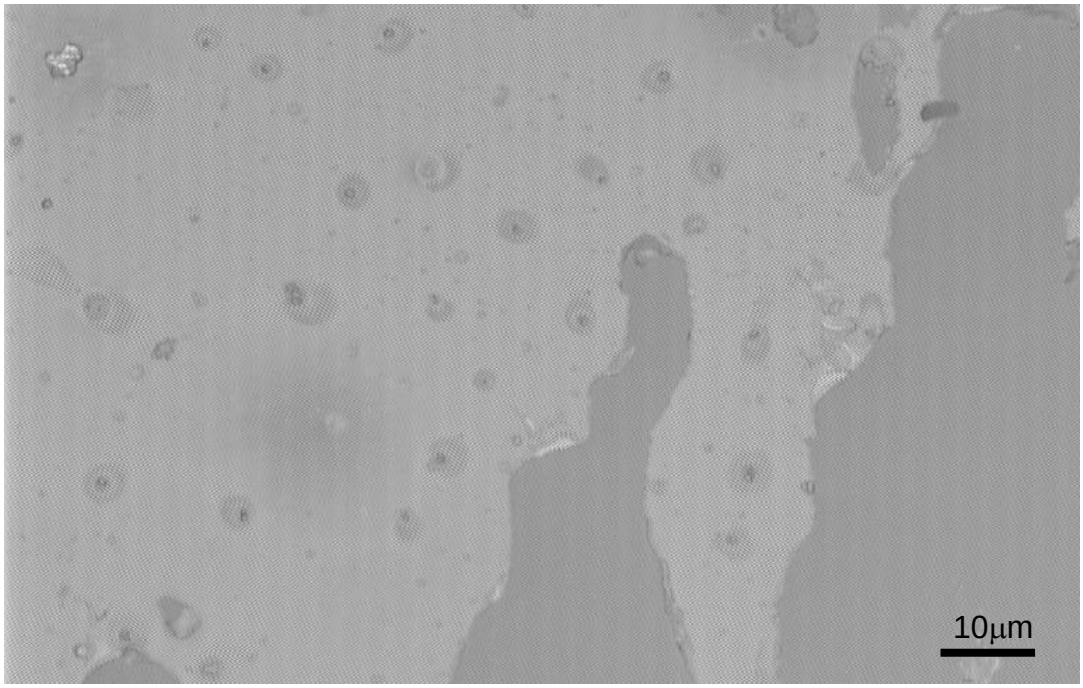

Fig. 8: Reflected light micrograph showing defects in the Ag/ZnO interfaces revealed in a simulated transit scratch in Pilkington Optitherm.